Validation of DWI pre-processing procedures for reliable differentiation between human brain gliomas

Sebastian Vellmer[1,*], **Aram S. Tonoyan**[2], **Dieter Suter**[1], **Igor N. Pronin**[2], **Ivan I. Maximov**[1,**]

[1] Experimental Physics III, TU Dortmund University, Dortmund, Germany
[2] Burdenko Neurosurgery Institute, Moscow, Russia

Received 8 November 2016; accepted 20 April 2017

Abstract

Diffusion magnetic resonance imaging (dMRI) is a powerful tool in clinical applications, in particular, in oncology screening. dMRI demonstrated its benefit and efficiency in the localisation and detection of different types of human brain tumours. Clinical dMRI data suffer from multiple artefacts such as motion and eddy-current distortions, contamination by noise, outliers etc. In order to increase the image quality of the derived diffusion scalar metrics and the accuracy of the subsequent data analysis, various pre-processing approaches are actively developed and used. In the present work we assess the effect of different pre-processing procedures such as a noise correction, different smoothing algorithms and spatial interpolation of raw diffusion data, with respect to the accuracy of brain glioma differentiation. As a set of sensitive biomarkers of the glioma malignancy grades we chose the derived scalar metrics from diffusion and kurtosis tensor imaging as well as the neurite orientation dispersion and density imaging (NODDI) biophysical model. Our results show that the application of noise correction, anisotropic diffusion filtering, and cubic-order spline interpolation resulted in the highest sensitivity and specificity for glioma malignancy grading. Thus, these pre-processing steps are recommended for the statistical analysis in brain tumour studies.

Keywords: Diffusion MRI, Pre-processing schemes, Noise correction, Data smoothing algorithm, Spatial interpolation, Glioma differentiation

1 Introduction

Diffusion weighted magnetic resonance imaging (dMRI) is a powerful modern imaging modality in research and clinical applications that allows one to efficiently probe and visualise the structure and function of the human anatomy *in vivo*. In particular, human brain studies actively exploit the capabilities of dMRI to detect, localise and estimate the degree of injury for different brain diseases such as stroke [1,2], traumatic brain injuries [3,4], and, especially, neurooncology [5–8]. The striking peculiarity of dMRI is the ability to exploit the motion of water molecules on the micrometer scale and to convert obtained information into a meaningful image [9]. However, the simplified visualisation of neuronal tissue, such as diffusion tensor imaging (DTI), found widespread applications [10] whereas the accurate theoretical description of biophysical models of water diffusion in biological tissue is still puzzling and remains a challenging problem [11].

Different approaches exist for the interpretation of the diffusion signal attenuation. The simplest and most often used approach is to fit the signal decay using mono-exponential function. In this case one can describe the behaviour of water diffusion by a second-order symmetric tensor **D**. Its elements can be determined by measuring the apparent diffusion

* Corresponding author: Sebastian Vellmer, Experimental Physics III, TU Dortmund University, Dortmund, Germany
** Corresponding author: Ivan I. Maximov, Experimental Physics III, TU Dortmund University, Dortmund, Germany
E-mail addresses: vellmer@e3.physik.tu-dortmund.de (S. Vellmer), ivan@e3.physik.tu-dortmund.de (I.I. Maximov).

coefficients in at least six non-coplanar directions. Alternatively, a cumulant expansion of the signal decay allows one to take into account second order effects, specifically the so-called apparent kurtosis coefficient [12,13] and reconstruct diffusion kurtosis tensor. Tensor-based approaches allow us to reconstruct either the symmetric second order diffusion tensor, using 6 non-coplanar diffusion directions or complementary the fourth-order symmetric diffusion kurtosis tensor (also known as diffusion kurtosis imaging (DKI)) by acquiring 15 diffusion directions. Well known limitations of the tensor based approaches such as the difficulties in explanation of the underlying microstructure motivated further attempts to describe the diffusion process in terms of biophysical model. One of the promising and popular models is neurite orientation dispersion and density imaging (NODDI) [14]. In order to model the axon bundle NODDI uses a bunch of zero-radius cylinders with impermeable cylinder walls, i.e. one assumes that diffusion in the perpendicular direction to the axon axis is negligible. The directional dispersion of the axonal bundle can be described by the orientation distribution Watson or Bingham functions [14,15]. Thus, NODDI allows us to describe water behaviour in three principle diffusion compartments, namely, intra- and extra-axonal spaces, and free water pool. Therefore, the NODDI model already found multiple applications in neuroimaging [16–18] and still keeps evolving.

The derived scalar metrics of diffusion approaches such as DTI or DKI are extensively used in neurooncology studies [7,8,17], for example, in glioma grade differentiation [5,19]. The World Health Organisation (WHO) divides the glioma grades into four groups [20] according to their malignancy. Reliable glioma differentiation is a critical procedure for the selection of treatment strategies, evaluation of radiochemotherapy, and prognosis of survival rates. The "gold standard" in the glioma grading is still based on histological and immunohistochemical features of the tumour such as cellular atypia, proliferating index, miotic activity, and the presence of necrosis. The grading examination often requires invasive procedures such as biopsy or surgical resection with associated risks. In contrast, dMRI offers a non-invasive alternative, with the potential to perform the glioma malignancy differentiation using diffusion scalar metrics provided by the chosen diffusion approach [5,7,8].

It is known that accuracy and precision of diffusion metrics strongly depend on the details of the workflow [21–26]. Thus, all typical steps in raw data pre-processing such as noise correction, motion and eddy-current corrections, smoothing of diffusion data and applied estimation algorithms are very important and may impact the subsequent analysis. Unfortunately, to the best of our knowledge, there is no systematic comparison of the pre-processing approaches for the case of glioma differentiation. In the present work, we show effects of different pre-processing steps on the glioma grading problem using the biomarkers derived from DTI, DKI and NODDI. As the result of this study, we determine the most reliable pre-processing workflow, which can be a powerful complement for clinical use.

2 Methods and materials

The study was approved by the Burdenko Neurosurgery institutional ethics committee. Written informed consent was obtained from all patients. 24 patients with supratentorial gliomas were enrolled in the study. All patients had undergone MRI screening at the Burdenko Neurosurgery Institute where they were treated. All gliomas were newly diagnosed, without any radiation, surgery or chemotherapy treatments. Patients with different oncological history were excluded. All patients underwent tumour removal or stereotactic biopsy 1-2 weeks after the MRI examination. The diagnosis of glioma and WHO grade were confirmed by histology and immunohistochemical examination in all cases. According to the generally accepted approach [20], the gliomas were categorised into glioma grades II, III, and IV. The study included 16 patients with high grade glioma (HGG) (8 patients with glioma-IV and 8 patients with glioma-III) and 8 patients with low grade glioma (LGG) (8 patients with glioma-II). The group of patients with glioma-IV consisted of the subjects with glioblastoma. The group of patients with glioma-III consisted of 8 subjects with anaplastic astrocytoma. The group of patients with glioma-II consisted of 8 subjects with diffuse fibrillary astrocytoma. The study included 16 males and 8 female patients in the age range from 18 to 59 years.

All patients underwent MRI examination with a 3 T GE scanner using a diffusion-weighted spin-echo echo-planar imaging sequence with three b-values 0, 1000, and 2500 s/mm^2 and 60 non-coplanar diffusion gradient directions for each non-zero b-value. Other diffusion protocol parameters were: repetition time (TR) = 10000 ms; echo time (TE) = 103.4 ms; field of view (FoV) = 240 × 240 mm^2; matrix-size 80 × 80; slice thickness 3 mm; intersection gap 0 mm; total number of slices 32; number of excitation (NEX) = 1; total acquisition time 22 min. Additionally, we acquired anatomical reference images: T_2-weighted images (TR = 4300 ms; TE = 85 ms; turbo factor = 21; FoV = 240 × 240 mm^2; matrix-size = 512 × 512; slice thickness = 3 mm; intersection gap = 0 mm; NEX = 2); T_2-FLAIR-weighted images (TR = 9500 ms; TE = 120 ms; inversion time (TI) = 2250 ms; FoV = 240 × 240 mm^2; matrix = 352 × 325; slice thickness = 5 mm; intersection gap = 0 mm; NEX = 1). T_1-weighted images were recorded with and without Gd contrast agent (0.1 mmol/kg), using the parameters TR = 875 ms; TE = 85 ms; FoV = 240 × 240 mm^2; matrix-size = 384 × 384, slice thickness = 3 mm, intersection gap = 0 m; NEX = 2.

Prior to any estimations of the diffusion scalar metrics, the original raw diffusion data were corrected for eddy-current distortions and motion artefacts using coregistered affine transformations with the mutual information as a quality criterion. The coregistration procedure was implemented in the

ElastiX software [27] and later visually inspected for high b-values. The diffusion gradient directions were corrected with the same transformations, using in-house Matlab scripts (MATLAB, The MathWorks, Natick, MA USA) [22].

We divided the data sets into five groups:

- **Data 1**: raw data without any additional processing;
- **Data 2**: diffusion data with applied noise correction using the non-central χ^2 distribution [28]:

$$P(S,\sigma,L)=\frac{A_L^{L-1}}{\sigma^2}S^L e^{-\frac{S^2+A_L^2}{2\sigma^2}} I_{L-1}\left(\frac{A_L S}{\sigma^2}\right)u(S), \qquad (1)$$

  where L is the number of coils used for parallel imaging, σ^2 is the noise variance, and $I_L(\cdot)$ is the Lth order Bessel function of the first kind and $u(\cdot)$ is the Heaviside step function; $A_L(x)=\sqrt{\sum_i^L |A^2(x)|^2}$. Each diffusion weighted image was a subject for noise correction separately;
- **Data 3**: filtered Data 2 with 3D Gaussian smoothing kernel of 1.5 mm^3 implemented in Convert3D utility [29]; After a step 2, each diffusion weighted image was a subject for the Gaussian filter in prior to any diffusion metric estimation. It is important difference in our pre-processing steps, i.e. conventionally, the smoothing algorithm is applied to the final diffusion metrics directly.
- **Data 4**: Data 2 with anisotropic diffusion filtering based on the Perona-Malik algorithm [30] with the conductance of 0.8 and 100 iterations implemented in the Convert3D utility [29]. In contrast to the Gaussian filter the anisotropic diffusion smoothing allows one to keep the boundaries between image contrasts, i.e. to produce less blurring data. An application of Perona-Malik filter was performed in prior to any diffusion metric estimation.
- **Data 5**: a third order spline interpolation was applied to Data 2, using the Convert3D utility [29] in addition to the anisotropic diffusion filter based on the Perona-Malik algorithm. As a result, we obtained a higher spatial resolution of $1.5\times1.5\times1.5$ mm^3. This interpolation is an important step for further finer tumour delineation and masking [31]. Note, that pre-processing corrections were done separately to each diffusion weighted image in prior to any scalar metric estimation.

In the case of DTI the diffusion signal attenuation S is described by mono-exponential function: $\ln(S/S_0)=-b\cdot D_a$, where S_0 is the signal without diffusion weighted gradients, D_a is the apparent diffusion coefficient [9] and b is the diffusion weighting (so-called b-value). The diffusion tensor elements can be determined by measuring the apparent diffusion in at least six non-coplanar directions $\vec{n}$, with $\ln(S_n/S_0)=-b\,\vec{n}\cdot\mathbf{D}\cdot\vec{n}$. In turn, the cumulant expansion of the signal decay DKI describes the quadratic effect as a function of $b\cdot D_a$ [12,13]:

$$\ln\left(\frac{S}{S_0}\right)=-b\cdot D_a+\frac{1}{6}(b\cdot D_a)^2\cdot K_a, \qquad (2)$$

where K_a is the apparent kurtosis value. To estimate the full fourth-order kurtosis tensor at least 15 diffusion directions are demanded.

In order to describe the underlying microstructure, NODDI model exploits a decomposition of the diffusion signal into three terms [14,32]:

$$\frac{S}{S_0}=(1-\nu_{iso})(\nu_a\cdot S_a+(1-\nu_a)S_e)+\nu_{iso}\cdot S_{iso}, \qquad (3)$$

where S_a is the signal of the intra- and S_e of the extra-axonal spaces, respectively, S_{iso} is the signal of the isotropic water compartment. The fractions of the compartments are presented **by ν_a as the intra-axonal fraction and ν_{iso} as the fraction of free water. The normalised diffusion signals of intra- and extra-axonal spaces depends on the mutual orientation of axon bundle $\vec{n}$ and diffusion encoding direction $\vec{q}$**[14]:

$$S_a=\int_{S^2} f(\vec{n})e^{-bD_a\cdot(\vec{q}\cdot\vec{n})^2}d\vec{n} \qquad (4)$$

$$\log S_e=-b\cdot\vec{q}^T\cdot\left(\int_{S^2} f(\vec{n})D(\vec{n})d\vec{n}\right)\cdot\vec{q}, \qquad (5)$$

where $D(\vec{n})$ is the cylindrically symmetric tensor with the principle direction of diffusion $\vec{n}$, diffusion coefficients $d_\parallel=D_a$ parallel to $\vec{n}$ and $d_\perp=D_a\cdot(1-\nu_a)$ perpendicular to $\vec{n}$; D_a is the intrinsic diffusion coefficient along the axon. The orientation distribution function $f\colon S^2\to R$ describing the axonal dispersion based on a Watson distribution is:

$$f(\vec{n})=M\left(\frac{1}{2};\frac{3}{2};\kappa\right)^{-1}\exp\left(\kappa(\vec{\mu}\cdot\vec{n})^2\right), \qquad (6)$$

where M is a confluent hypergeometric function, $\vec{\mu}$ is the mean axon orientation, and κ is the concentration parameter that measures the extent of orientation dispersion about $\vec{\mu}$ [14,32]. The orientation dispersion index (ODI) is defined as [32]

$$\mathrm{ODI}=\frac{2}{\pi}\arctan\left(\frac{1}{\kappa}\right), \qquad (7)$$

where ODI is limited by [0,1] range. Tract density (TD) and isotropic fraction (ISO) metrics are represented by appropriate fraction parameters ν_a and ν_{iso}, respectively, in Eq. (3).

In order to extract the NODDI model parameters a few important assumptions should be done: 1) intra-axonal and

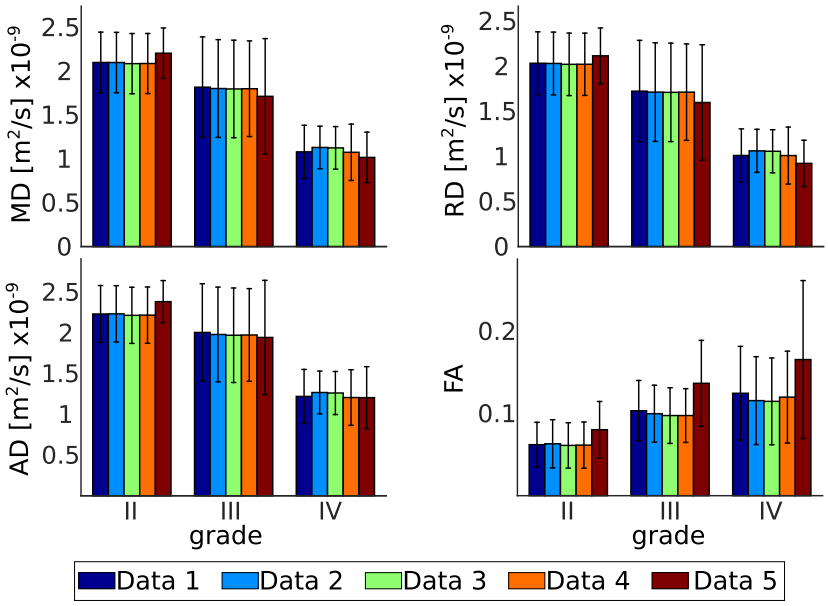

Figure 1. Averaged DTI metrics such as mean diffusivity (MD), radial diffusivity (RD), axial diffusivity (AD), and fractional anisotropy (FA) are presented. The colour bars are grouped for tumour grades II, III and IV, respectively.

extra-axonal diffusivities are equal: $D_a = d_{\parallel}^e$; 2) intra-axonal diffusivity is fixed $D_a = 1.7\mu m^2/ms$. As a result, the estimated parameters are ν_a, ν_{iso}, and κ. Note, that fitting of Eq. (3) demands a constraint optimisation algorithm recalling made assumptions for S_a, S_e, and S_{iso} signals [14]. In turn, in Ref. [33] authors have shown that the optimisation problem has two equivalent physically meaningful solutions. Therefore, it is impossible to predict to what kind of local minima the solution converges.

Complex diffusion models such as NODDI are computationally very demanding [33], in particular, for highly reproducible robust assessments of the diffusion metrics. To reduce the computational complexity, we divided the optimisation into two steps: the first estimation is a simple single start minimisation with the gradient descent algorithm. On the next stage we localised the ill-conditioned voxels where the ODI values are equal to 0.704833. In these voxels, the gradient descent algorithm has converged to a local minimum, as the result of non-optimal starting values for the NODDI model. In turn, the local convergence problem leads to flat contrast clusters in the scalar diffusion metrics, which can be easily identified. For these voxels, we changed the optimisation scheme to multi-start, with a stronger perturbation of the initial guesses obtained from the first step. As a result, the second step reduced the number of ill-conditioned voxels significantly.

The following DTI and DKI scalar metrics were estimated with ExploreDTI [34]: mean, radial, axial diffusivity (MD, RD, AD, respectively), fractional anisotropy (FA), mean, radial, axial kurtosis (MK, RK, AK, respectively), and anisotropy of kurtosis (KA). In order to reduce possible variability based on the applied estimation algorithm [25] we used a linear weighted algorithm. NODDI scalar metrics were derived from fitting of dMRI data following Eq. (3) and original Matlab toolbox[1].

The tumour masking for all subjects was performed using Data 4 and Data 5 independently by a trained neuroradiologist using the ITK-SNAP toolbox [29]. Regions of interests were drawn manually around the solid tumour parts with the highest values of MK metric in the tumour. The accuracy of the tumour masking was tested in accordance with T_1- and T_2-weighted images. Instead of using the whole heterogeneous region of the solid tumour, we assumed that a tissue with the highest tumour grade is localised within the area with the highest MK values [5,7,8]. In this manner at least three slices were masked for each patient.

All statistical tests were performed using in-house Matlab scripts and the Matlab statistical toolbox.

3 Results

In order to present the absolute values of all diffusion metrics depending on the glioma grades we averaged each scalar diffusion metric over all patients in the group. Averaged DTI metrics over all patients for each tumour grade group are presented in Fig. 1. Interestingly, all metrics decrease with increasing malignancy grade with the exception of the FA values. The non-interpolated Data 1–4 exhibit almost the same mean values and standard deviations in all metrics, in contrast to the Data 5.

[1] http://mig.cs.ucl.ac.uk/mig/mig/index.php/?n=Tutorial.NODDImatlab/

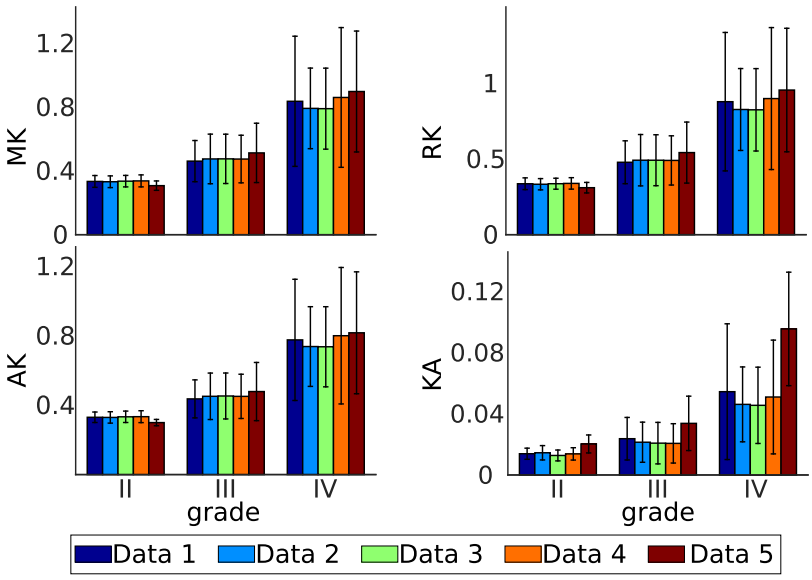

Figure 2. Averaged DKI metrics such as mean kurtosis (MK), radial kurtosis (RK), axial kurtosis (AK) and kurtosis anisotropy (KA) are presented. The colour bars are grouped for the tumour grades II, III and IV, respectively.

Averaged DKI metrics are presented in Fig. 2. Similar to the DTI metrics, all of the averaged metrics show a monotonous increase with glioma malignancy.

Averaged NODDI metrics are presented in Fig. 3. The scalar metrics from Data 5 differ strongly from the Data 1–4.

In order to answer the question: do different pre-processing approaches produce significantly different diffusion metrics inside of each glioma grade group, we performed Kruskal–Wallis tests [35] for the mean values of each diffusion metric. The statistical tests for all diffusion metrics were performed twice: first for all data sets and then for Data 1-4. The results of the tests are presented in Table 1. The significance criterion was $p < 0.05$. The H_0 hypothesis (no significant difference between mean values) was always accepted for the Data 1–4. The Kruskal-Wallis tests did not find a significant difference in all diffusion metrics with and without Data 5, except for KA values in glioma grade-II, TD and ODI metrics for glioma grade-II, and ISO values in glioma grade-IV by including Data 5.

In order to perform a glioma differentiation between three malignancy grades we applied the two-side pair Wilcoxon-Mann-Whitney tests. The diffusion values were

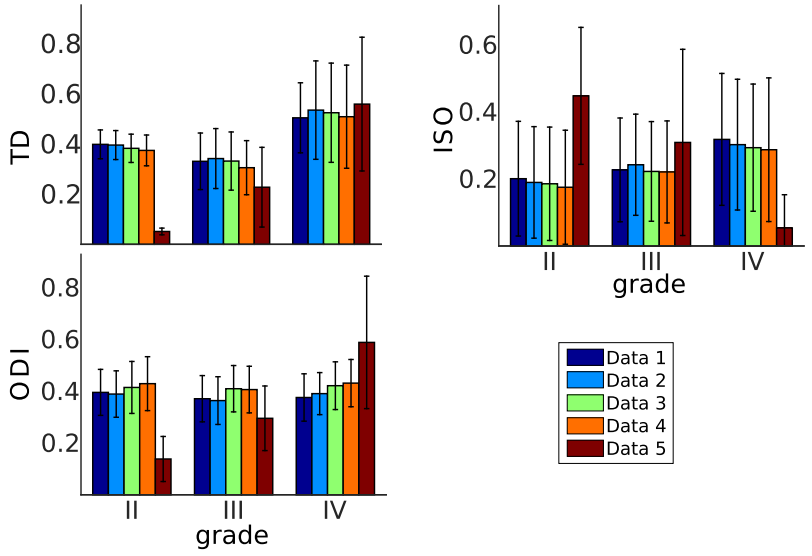

Figure 3. Averaged NODDI metrics such as tract density (TD), isotropic volume fraction (ISO) and orientation dispersion index (ODI). The colour bars are grouped for the tumour grades II, III and IV, respectively.

Table 1
Results of the Kruskal-Wallis tests within each glioma grade for the Data 1–4 and ex-/including Data 5. The crosses means that the H_0 hypothesis is accepted (no significant difference).

Metrics	Glioma grades					
	Without Data 5			With Data 5		
	II	III	IV	II	III	IV
MD	X	X	X	X	X	X
RD	X	X	X	X	X	X
AD	X	X	X	X	X	X
FA	X	X	X	X	X	X
MK	X	X	X	X	X	X
RK	X	X	X	X	X	X
AK	X	X	X	X	X	X
KA	X	X	X		X	X
TD	X	X	X		X	X
ISO	X	X	X	X	X	
ODI	X	X	X		X	X

Table 2
Results of the pair Whitney–Mann tests between different glioma grades for Data 1–V. The criterion of the significance is $p < 0.05$.

Scalar	Grade II vs III					Grade II vs IV				
Metrics	Data 1	Data 2	Data 3	Data 1V	Data 5	Data 1	Data 2	Data 3	Data 4	Data 5
MD	X	X	X	X	X					
RD	X	X	X	X	X					
AD	X	X	X	X	X					
FA										
MK										
RK										
AK										
KA	X	X	X	X	X					
TD	X	X	X	X			X	X	X	
ISO	X	X	X	X	X	X	X	X	X	
ODI	X	X	X	X		X	X	X	X	

scalar	Grade III vs IV					Grade LGG vs HGG				
Metrics	Data 1	Data 2	Data 3	Data 4	Data 5	Data 1	Data 2	Data 3	Data 4	Data 5
MD										
RD					X					
AD					X					
FA	X	X	X	X	X					
MK										
RK										
AK										
KA	X			X			X			
TD		X	X	X		X	X	X	X	
ISO	X	X	X	X	X	X	X	X	X	
ODI	X	X	X	X		X	X	X	X	

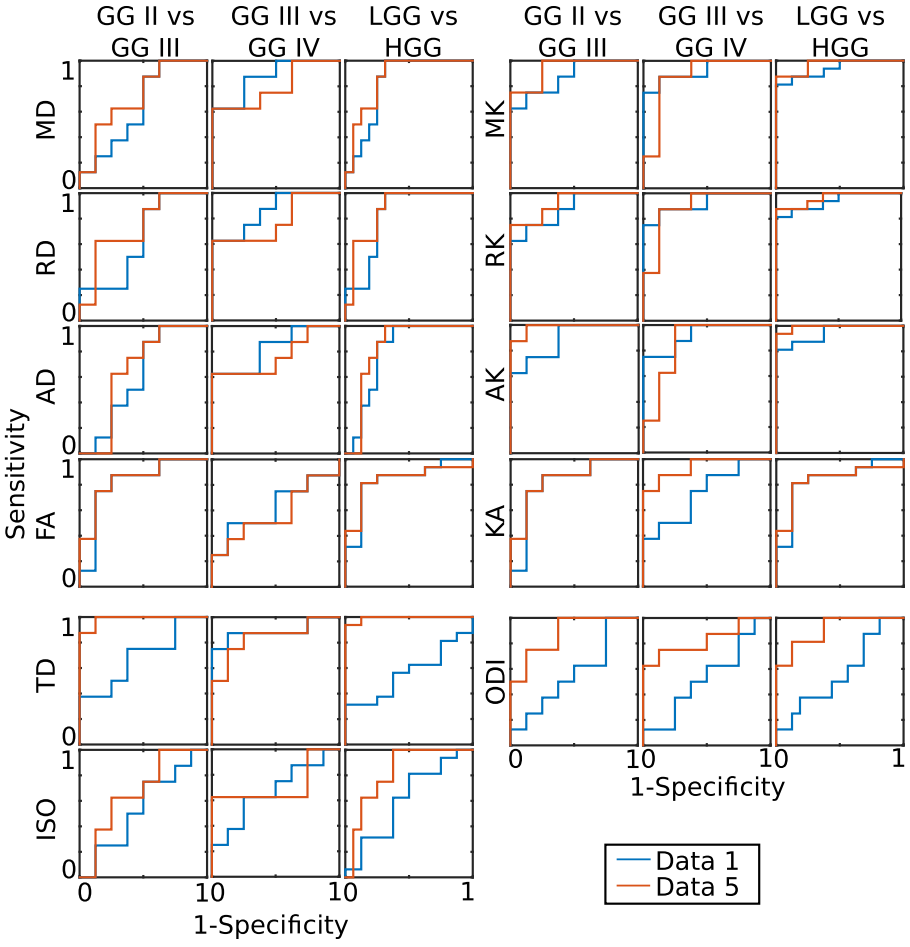

Figure 4. The ROC curves for Data 1 and V for glioma differentiation: glioma grade (GG) II vs III, GG III vs IV, and LGG vs HGG.

compared for grade-II vs grade-III, grade-II vs grad-IV, grade-III vs grade-IV, and LGG vs HGG. The criterion of significant difference was chosen $p < 0.05$. The results of the statistical tests are presented in Table 2. The cases, where H_0 hypothesis was not rejected, are marked by crosses. There are no significant differences determined between glioma grades II and III for MD, RD, AD, KA and ISO for all Data. For the metrics MK, RK and AK we detected a significant difference between all grades using all data sets. Surprisingly, Data 2, 3, and 4 could not detect a significant difference on the basis of TD, ISO, and ODI metrics between glioma grades II vs IV. In the case of LGG vs HGG in Data 1 we did not detected a significant difference for the NODDI scalar metrics. Data 5 allowed us to find significant differences between grades II vs IV, and LGG vs HGG for all diffusion metrics.

Since we did not find significant differences between Data 1–4 within each glioma grade group we decided to use Data 1 for further receiver operator characteristic (ROC) analysis together with Data 5. We applied ROC analysis [35] for all diffusion metrics derived from Data 1 and Data 5. The ROC curves are presented in Fig. 4. The related Area Under Curve (AUC) values are presented in Table 3. In five cases the AUC values are higher for the Data 1 compared to the Data 5. Notably, AUCs values for NODDI scalar metrics estimated within Data 5 are higher, for example, for TD metrics in LGG vs HGG: Data 1 (0.56)/Data 5 (0.99).

Using Data 1 and 5 we performed a comparison for the absolute diffusion values taken over all masked voxels, namely, MD, FA, MK, ISO, and ODI, for each glioma grade. The resulting histograms are presented in Fig. 5.

4 Discussion

In the present work we performed a statistical comparison between different pre-processing strategies for a glioma differentiation problem. Until now, a “gold pre-processing standard” for dMRI data, which allows one to process the raw diffusion data for optimal suppression of artefacts, could not be chosen. Moreover, recently it has been shown that the diffusion scalar metrics are very sensitive to many factors

Table 3
AUC values estimated from ROC analysis in Fig. 4.

Scalar Metrics	AUC values					
	Grade II vs III		Grade II vs IV		Grade LGG vs HGG	
	Data 1	Data 5	Data 1	Data 5	Data 1	Data 5
MD	0.64	0.72	0.88	0.8	0.82	0.86
RD	0.64	0.73	0.86	0.78	0.82	0.87
AD	0.61	0.66	0.86	0.78	0.80	0.83
FA	0.81	0.84	0.62	0.58	0.84	0.84
MK	0.88	0.94	0.92	0.88	0.94	0.97
RK	0.88	0.92	0.92	0.89	0.94	0.96
AK	0.89	0.98	0.92	0.86	0.95	0.99
KA	0.66	0.70	0.73	0.94	0.77	0.85
TD	0.69	0.98	0.89	0.84	0.56	0.99
ISO	0.55	0.67	0.67	0.72	0.61	0.82
ODI	0.56	0.88	0.53	0.83	0.56	0.91

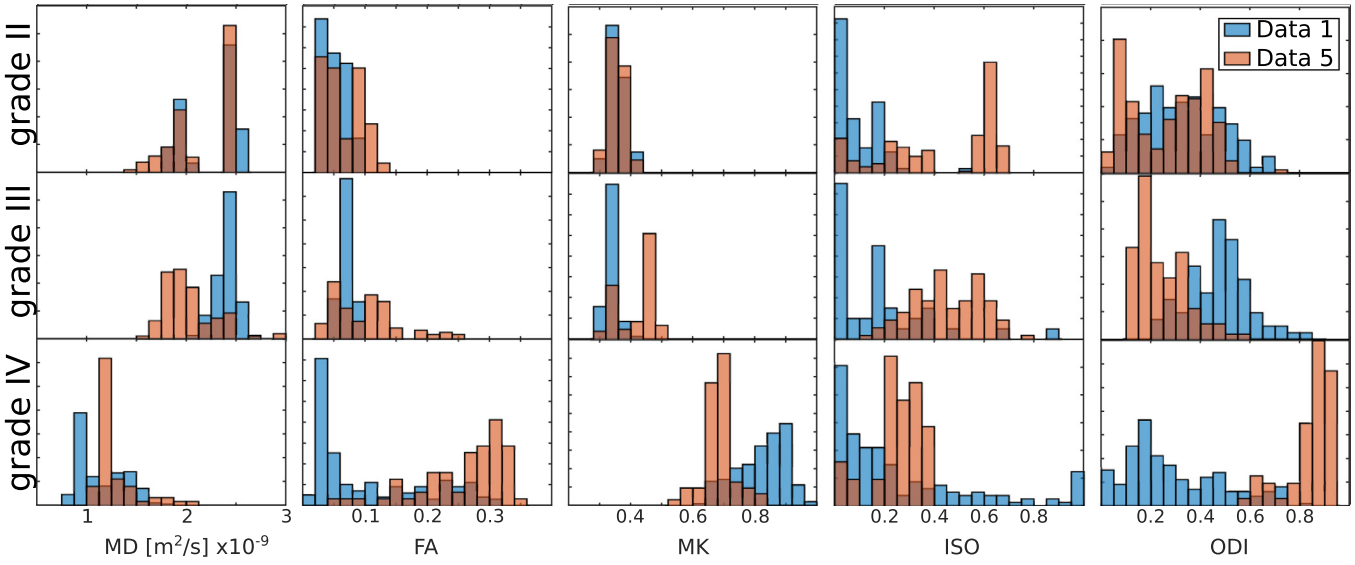

Figure 5. Histograms of the absolute values of the diffusion metrics (MD,FA,MK,ISO, and ODI) versus increasing glioma grade.

such as motion or eddy-current corrections [36], selection of a numerical algorithm for the scalar metrics derivation [25,37], influence of susceptibility distortions on the scalar metrics [38] and problems related to high diffusion weightings [39]. All these artefacts are able to influence the data analysis. As a consequence, optimised pre-processing workflows can significantly improve the selection of the next treatment, in particular, in the case of tumour studies.

In order to embrace most typical pre-processing steps we have chosen five typical operations. The first includes no any additional corrections apart from motion correction of the raw data. Noise correction is an important independent problem in MRI [28,40,41]. Correspondingly, the noise corrected Data are picked out in a separate group Data 2. In order to decrease the measurement time of diffusion measurements, parallel imaging is often used. As a consequence, the method developed by Aja-Fernandez and colleagues with application of the non-central χ^2 distribution is a very attractive noise correction algorithm [28,40]. After the noise correction, data filtering could be done by applying two typical smoothing techniques: the Gaussian smoothing (Data 3) and anisotropic diffusion filtering (Data 4). Note, that frequently the smoothing algorithm is applied to the estimated diffusion scalar metrics prepared to the subsequent statistical analysis. In contrast to that, we filtrated the original diffusion-weighted data.

So-called “super-resolution methods” have been developed for improving the image resolution without excessively

increasing the measurement time [42,43]. However, super-resolution approaches frequently demand additional acquisitions with non-isotropic voxel sizes. Alternatively, higher spatial resolution can be obtained at clinical scanners as a default option by a simple linear interpolation. It was already proven that accurate cubic spline interpolation leads to a significant improvement in the case of fibre tracking [31] and it might be exploited in the tumour studies as well. Thus, the Data 5 accumulated three important operations: the noise correction, anisotropic diffusion filtering based on Perona-Malik algorithm and cubic spline interpolation.

As shown by Figs. 1 and 2, the difference between all pre-processing approaches is very small. This result is confirmed by the Kruskal–Wallis tests (see Table 1) with and without Data 5. The largest difference between pre-processing steps was found in the case of the NODDI metrics when we added the Data 5 to the statistical tests. We conjecture that this significant discrepancy might be related to the numerical problems of the NODDI model itself [33], which uses a fixed set of parameters, whose values were determined from healthy tissue. Studies of tumours, like the present one, might require different parameter sets, possibly depending on the glioma grade. The higher spatial resolution produced by the spline interpolation of Data 5 introduced moderate bias in the NODDI scalar metrics. Nevertheless, Data 5 demonstrated its efficiency in the case of the pair Wilcoxon–Whitney–Mann tests (see Table 2). The two-side pair Wilcoxon–Whitney–Mann test between glioma grades-II and IV and LGG vs HGG found significant differences for all NODDI metrics in contrast to the Data 1-4. Notably, the DKI metrics are very sensitive in all glioma grade cases, independent of the pre-processing steps.

Since the non-interpolated Data 1-4 did not exhibit a significant difference between each other in the same glioma grade group, it is sufficient to compare Data 1 with 5 in order to estimate the sensitivity and specificity of the pre-processing approaches. The sensitivity and specificity of the Data 5 is much higher than for Data 1 for many diffusion metrics, in particular, for the NODDI values. One can find that the ROC curves (Fig. 4 and related AUC values Tab. 3) are higher for many metrics derived from Data 5. This result is most prominent in the comparison of LGG vs HGG. The analysis of the distance to the optimal operating point presented in Fig. 4 shows significant improvements of Data 5 compared to Data 1 for DKI and NODDI metrics.

The changes in the diffusion metrics (MD, FA, MK, ISO, ODI) depending on the glioma grade are presented in Fig. 5. For grade II, all diffusion metrics coincide for Data 1 and 5 except of ISO. A significant difference between derived metrics from Data 1 and 5 can be observed in the case of grade IV except for MD. In turn, the Data 5 demonstrated significant quantitative changes along the grades in contrast to the Data 1.

The most important limitation of our study is the small number of patients per group. Small number of patients reduces the statistical power of the obtained prediction. However, we have to point that in the case of our study in each group we selected only the gliomas with the same type of tumour morphology such as diffuse fibrillary astrocytoma, anaplastic astrocytoma, and glioblastoma for grades II, III, and IV, respectively. It is very well known that even in the case of the same glioma grade the location, tumourgenesis and morphology of the tumour are important covariances. Thus, in order to increase the reliability of the analysis and to introduce additional covariates, in particular, for the NODDI metrics, we need to acquire data from a larger number of patients. Next limitation is an accuracy of scalar metrics derived from the interpolated data. The applied spline interpolation algorithm introduced smooth signal variations into the original data. However, the diffusion weighted datasets represent complex mutually connected structures such as defined semi-positive diffusion tensors, conjugated bundle distribution inside of the voxels. The direct interpolation in the regions with a strong signal variability might introduce unaccounted bias in the resulting metrics. Besides of this, applied diffusion models could be numerically unstable in sense of the scalar metric assessments such as, for example, the NODDI. Thus, the interpolation procedure should be performed carefully, probably, taking into account additional regularisation parameters [44].

5 Conclusion

The pre-processing approach exploiting a noise correction, anisotropic diffusion filtering, and cubic spline interpolation to the raw diffusion data allowed us to increase statistical reliability of the glioma grade differentiation, in particular, in the cases of grade-II vs grade-III and grade-III vs grade-IV. Independently of the pre-processing steps, we verified a very high potential in the malignancy grading exhibited the metrics based on the DKI derived values which can be improved by the cubic spline interpolation. The NODDI scalar metrics such as tract density and orientation dispersion index in the case of interpolated diffusion data demonstrated high sensitivity for glioma differentiation between high and low grade gliomas. We can recommend the cubic spline interpolation approach for the further statistical analysis in the brain tumour studies as a useful complementary method for all clinical studies.

Acknowledgement

The work was financially supported by the DFG grant SU 192/32-1 and RSF grant 14-15-00197. Authors thank the ITMC of TU Dortmund University for an accessible computational facility.

References

[1] Hui ES, Du F, Huang S, Shen Q, Duong TQ. Spatiotemporal dynamics of diffusional kurtosis, mean diffusivity and perfusion changes in experimental stroke. Brain Res 2012;1451:100–9.

[2] Schlaug G, Siewert B, Benfield A, Edelman R, Warach S. Time course of the apparent diffusion coefficient (ADC) abnormality in human stroke. Neurology 1997;49(1):113–9.

[3] Kou Z, VandeVord PJ. Traumatic white matter injury and glial activation: from basic science to clinics. Glia 2014;62:1831–55.

[4] Hannawi Y, Stevens RD. Mapping the connectome following traumatic brain injury. Curr Neurol Neurosci Rep 2016;16:44.

[5] Raab P, Hattingen E, Franz K, Zanella FE, Lanfermann H. Cerebral gliomas: diffusional kurtosis imaging analysis of microstructural differences. Radiology 2010;254(3):876–81.

[6] Goebell E, Paustenbach S, Vaeterlein O, Ding XQ, Heese O, Fiehler J, Kucinski T, Hagel C, Westphal M, Zeumer H. Low-grade and anaplastic gliomas: differences in architecture evaluated with diffusion-tensor MR imaging. Radiology 2006;239:217–22.

[7] Van Cauter S, Veraart J, Sijbers J, Peeters RR, Himmelreich U, De Keyzer F, Van Gool SW, Van Calenbergh F, De Vleeschouwer S, Van Hecke W, Sunaert S. Gliomas: diffusion kurtosis MR imaging in grading. Radiology 2012;263:492–501.

[8] Jiang R, Jiang J, Zhao L, Zhang J, Zhang S, Yao Y, Yang S, Shi J, Shen N, Su C, Zhang J, Zhu W. Diffusion kurtosis imaging can efficiently assess the glioma grade and cellular proliferation. Oncotarget 2015;6:42380–93.

[9] Basser PJ, Mattiello J, LeBihan D. MR diffusion tensor spectroscopy and imaging. Biophys J 1994;66(1):259.

[10] Jones DK. Diffusion MRI: Theory, Methods, and Applications. Oxford University Press; 2010.

[11] Novikov DS, Jensen JH, Helpern JA, Fieremans E. Revealing mesoscopic structural universality with diffusion. Proc Natl Acad Sci USA 2014;111:5088–93.

[12] Jensen JH, Helpern JA, Ramani A, Lu H, Kaczynski K. Diffusional kurtosis imaging: the quantification of non-Gaussian water diffusion by means of magnetic resonance imaging. Magnet Reson Med 2005;53(6):1432–40.

[13] Jensen JH, Helpern JA. MRI quantification of non-Gaussian water diffusion by kurtosis analysis. NMR Biomed 2010;23(7):698–710.

[14] Zhang H, Schneider T, Wheeler-Kingshott CA, Alexander DC. NODDI: practical in vivo neurite orientation dispersion and density imaging of the human brain. Neuroimage 2012;61(4):1000–16.

[15] Tariq M, Schneider T, Alexander DC, Gandini Wheeler-Kingshott CA, Zhang H. Bingham-NODDI: mapping anisotropic orientation dispersion of neurites using diffusion MRI. Neuroimage 2016;133: 207–23.

[16] Daducci A, Canales-Rodríguez EJ, Zhang H, Dyrby TB, Alexander DC, Thiran JP. Accelerated microstructure imaging via convex optimization (AMICO) from diffusion MRI data. Neuroimage 2015;105:32–44.

[17] Wen Q, Kelley DA, Banerjee S, Lupo JM, Chang SM, Xu D, Hess CP, Nelson SJ. Clinically feasible NODDI characterisation of glioma using multiband EPI at 7t. Neuroimage Clin 2015;9:291–9.

[18] Sepehrband F, Clark KA, Ullmann JF, Kurniawan ND, Leanage G, Reutens DC, Yang Z. Brain tissue compartment density estimated using diffusion-weighted MRI yields tissue parameters consistent with histology. Hum Brain Mapping 2015;36:3687–702.

[19] Tietze A, Hansen MB, Østergaard L, Jespersen SN, Sangill R, Lund TE, Geneser M, Hjelm M, Hansen B. Mean diffusional kurtosis in patients with glioma: initial results with a fast imaging method in a clinical setting. Am J Neuroradiol 2015;36:1472–8.

[20] Louis DN, Ohgaki H, Wiestler OD, Cavenee WK, Burger PC, Jouvet A, Scheithauer BW, Kleihues P. The 2007 WHO classification of tumours of the central nervous system. Acta Neuropathol 2007;114:97–109.

[21] Moraschi M, Hagberg GE, Paola MD, Spalletta G, Maraviglia B, Giove F. Smoothing that does not blur: effects of the anistropic approach for evaluating diffusion tensor imaging data in the clinic. J Magnet Reson Imaging 2010;31:690–7.

[22] Leemans A, Jones D. The b-matrix must be rotated when correcting for subject motion in DTI data. Magnet Reson Med 2009;62:1336–49.

[23] Szczepankiewicz F, Lätt J, Wirestam R, Leemans A, Sundgren P, van Westen D, Stahlberg F, Nilsson M. Variability in diffusion kurtosis imaging: impact on study design, statistical power and interpretation. Neuroimage 2013;76:145–54.

[24] André ED, Grinberg F, Farrher E, Maximov II, Shah NJ, Meyer C, Jaspar M, Muto V, Phillips C, Balteau E. Influence of noise correction on intra- and inter-subject variability of quantitative metrics in diffusion kurtosis imaging. PLoS ONE 2014;9:e94531.

[25] Maximov II, Thönneßen H, Konrad K, Amort L, Neuner I, Shah NJ. Statistical instability of TBSS analysis based on DTI fitting algorithm. J Neuroimaging 2015;25:883–91.

[26] Maximov II, Grinberg F, Shah NJ. Robust tensor estimation in diffusion tensor imaging. J Magnet Reson 2011;213:136–44.

[27] Klein S, Staring M, Murphy K, Viergever MA, Pluim JPW. elastix: a toolbox for intensity based medical image registration. IEEE Trans Med Imaging 2010;29:196–205.

[28] Aja-Fernandez S, Tristan-Vega A, Hoge S. Statistical noise analysis in GRAPPA using a parametrized non-central chi approximation model. Magnet Reson Med 2011;65:1195–206.

[29] Yushkevich PA, Piven J, Hazlett HC, Smith RG, Ho S, Gee JC, Gerig G. User-guided 3D active contour segmentation of anatomical structures: significantly improved efficiency and reliability. Neuroimage 2006;31(3):1116–28.

[30] Perona P, Malik J. Scale-space and edge detection using anisotropic diffusion. IEEE Trans Pattern Anal Mach Intell 1990;12(7): 629–39.

[31] Dyrby TB, Lundell H, Burke MW, Reislev NL, Paulson OB, Ptito M, Siebner HR. Interpolation of diffusion weighted imaging datasets. NeuroImage 2014;103:202–13.

[32] Zhang H, Hubbard PL, Parker GJM, Alexander DC. Axon diameter mapping in the presence of orientation dispersion with diffusion MRI. Neuroimage 2011;56:1301–15.

[33] Jelescu IO, Veraart J, Fieremans E, Novikov DS. Degeneracy in model parameter estimation for multi-compartmental diffusion in neuronal tissue. NMR Biomed 2016;29(1):33–47.

[34] Leemans A, Jeurissen B, Sijbers J, Jones D. ExploreDTI: a graphical toolbox for processing, analyzing, and visualizing diffusion MR data. Proc Soc Magnet Reson Med 2009;17:3537.

[35] Vidakovic B. Statistics for bioengineering sciences: with MATLAB and WinBUGS support. Springer Science & Business Media; 2011.

[36] Graham MS, Drobnjak I, Zhang H. Realistic simulation of artefacts in diffusion MRI for validating post-processing correction techniques. Neuroimage 2016;125:1079–94.

[37] I. Maximov, F. Grinberg, I. Neuner, N. J. Shah, Robust diffusion imaging framework for clinical studies (2015) arXiv:1502.04967 [physics.med-ph].

[38] Andersson JL, Sotiropoulos SN. An integrated approach to correction for off-resonance effects and subject movement in diffusion MR imaging. Neuroimage 2016;125:1063–78.

[39] Nilsson M, Szczepankiewicz F, van Westen D, Hansson O. Extrapolation-based references improve motion and eddy-current correction of high b-value DWI data: application in parkinson's disease dementia. PLoS ONE 2015;10:e014182.

[40] Aja-Fernandez S, Vegas-Sanchez-Ferrero G, Tristan-Vega A. Noise estimation in parallel MRI: GRAPPA and SENSE. Magnet Reson Imaging 2014;32:281–90.

[41] Aja-Fernandez S, Brion V, Tristan-Vega A. Effective noise estimation and filtering from correlated multiple-coil MR data. Magnet Reson Imaging 2013;31:272–85.

[42] Coupe P, Manjon JV, Chamberland M, Descoteaux M, Hiba B. Collaborative patch-based super-resolution for diffusion-weighted images. Neuroimage 2013;83:245–61.

[43] Barajas RFJ, Hess CP, Phillips JJ, Von Morze CJ, Yu JP, Chang SM, Nelson SJ, McDermott MW, Berger MS, Cha S. Super-resolution track density imaging of glioblastoma: histopathologic correlation. Am J Neuroradiol 2013;34:1319–25.

[44] Castano-Moraga CA, Rodriguez-Florido MA, Alvarez L, Westin CF, Ruiz-Alzola J. Anisotropic interpolation of DT-MRI. Lecture Notes Comput Sci 2004;3216:343–50.